Chapter 9

Ion Exchange and Application of Layered Silicate

Kyeong-Won Park

Additional information is available at the end of the chapter

http://dx.doi.org/10.5772/51564

1. Introduction

Layered Na^+-titanosilicate ($Na_4Ti_2Si_8O_{22}{\cdot}4H_2O$) [1-5] has interesting potential applications. It contains titanosilicate layers composed of tetrahedral SiO_4 units and square pyramidal TiO_5 polyhedral [3]. The interlayer surfaces are composed of five-coordinated titanium (IV), and thus, are less coordinated than the octahedrally-coordinated microporous and layered titanosilicates [5]. The existence of five-coordinated titanium (IV) in interlayer surface makes Na^+-titanosilicate a promising material for oxidation catalysis. Each layer is separated by water molecules solvated around interlayer Na^+ ions [4]. Furthermore, this layer structure allows the intercalation of large organic and inorganic molecules.

Roberts et al. [3] synthesized Na^+-titanosilicate using Ti-alkoxide, and Ferdov and co-workers [5] described an effective means of producing Na^+-titanosilicate using $TiCl_4$ as a titanium source without an organic template. Kostov-kytin and co-workers [6] also investigated on the phase transition of Na^+-titanosilicate during heating at 300-700 ^oC. However, studies of Na^+-titanosilicate are still in the early stage. For industrial applications, in which Na^+-titanosilicate is used as a catalytic support, studies on surface chemistry, surface area, and porosity are needed, and on the relations between its surface properties and basic intercalation chemistry.

The galleries are normally occupied by exchangeable cations such as Na^+, Ca^{2+}, and Mg^{2+}. They happen easily an ion exchange reaction with quaternary ammonium ions or other organic cation in water [7]. The acid treatment of Na^+-titanosilicate can also produce Si-OH groups in interlayer surface by an ion exchange of exchangeable cations for H^+. Si-OH groups can offer an excellent bonding site for an organic base or alkoxysilane compound.

Pillaring of metal oxides in layered silicate, such as, natural and synthetic layered silicate is being increasingly studied [8–13]. In general, pillaring is achieved by the direct introduction of bulk inorganic (polyoxocations) or organic precursors (metal alkoxides) between the interlayers of layered silicate. Pillaring processes that use metal alkoxide are facilitated by a

preswelling step where by interlayer regions are exposed to quaternary ammonium [8,9,13]. However, preswelling procedures are problematic because they are complex, non-quantitative and require reagents. Recently, we reported a method of introducing metal alkoxides or organic precursors into H^+-layered silicates without a preswelling step [14–18].

Layered materials have been often used to design and construct organic–inorganic nanomaterials because of the ease and variety of modifications possible by the introduction of organic and inorganic compounds into the interlayer space [19–27]. In recent years, the chemical modification into the interlayer surface of layered materials has become the focus of increased research. Ruiz-Hitzky and Rojo [28,29] grafted trimethylsilyl groups to the interlayer silanol groups of H^+-magadiite starting with intercalation compounds from polar organic molecules. Shimojima et al.[30], Okutomo et al. [31], Ogawa et al. [32] and Yanagisawa et al. [33] reported on the trimethylsilylation, diphenylmethylsilylation and octyldimethylsilylation of magadiite, kenyaite and kanemite using the quaternary ammonium-exchanged form of silicates as intermediates. Thiesen et al. [34] also reported on the silylation of H^+-kenyaite using alkylamines together with a silylating agent.

We now report on the silylation of organic functional groups in the interlayer surface of a layered material. Functional organo-layered silicates with a functional group silylate in the interlayer surface can offer new opportunities for designing nanocomposites with the desired function because of their highly accessible interactions with various chemicals. In polymer–clay nanocomposite, physical properties depend on the interaction between exfoliated clay surfaces and the polymer. Interlayer surfaces bonded chemically by functional groups can interact with active groups in the polymer [35]. In particular, attached amine groups in the surface can chemically bond with epoxy [36], nylon [37], and urethane polymers [38], creating a bridge between the exfoliated layered surface and the polymer [35]. Their expanded gallery of functional groups can also store expensive reagents, such as drugs or enzymes. Layered materials with attached amine groups may be used to adsorb heavy metal ions for photosensitive species.

Here, we found that the H^+-titanosilicate (formed by proton exchange of Na^+-titanosilicate) produced H^+-titanosilicate/DDA (dodecylamine)/TEOS (tetraethylorthosilicate) intercalation compounds in DDA–TEOS solution. In these intercalation compounds, the long chain amine DDA appears to act as a gallery height expander and as a base catalyst during TEOS hydrolysis. Furthermore, it also appears to act as a liquid crystal template that forms surfactant-like molecular assemblies in galleries. The physical properties of the SPT derivatives produced were investigated by XRD (powder X-ray diffraction), BET (Brunauer, Emmett and Teller)-surface area, and SEM (scanning electron micrographs), and these investigations confirmed that SPT derivatives are mesoporous materials with large surface areas, highly ordered gallery structures, and high thermal resistances.

Intercalation and silylation were easily achieved by entropy differences between the interlayer gallery and the outside, which were caused by vaporizing the relatively more volatile ethanol. The ethanol on the outside vaporizes more rapidly than that in the interlayer gallery. DDA can also have a role as gallery expander and silylation catalyst.

Ethanol can quantitatively control the amount of OTES (octyltriethoxysilane) and DDA needed for gallery silylation, and the residual water from vaporization catalyzes the silylation reaction. This process was achieved by a quantitative procedure under atmospheric conditions without consumption of expensive reagents or an effluence of waste liquid. Our method is a promising route in leading to the preparation of new functional nanomaterials to bond with a variety of functional groups in the interlayer surface of layered materials.

2. Experimental section

2.1. Synthesis of Na^+-titanosilicate and H^+-titanosilicate

Na^+-tanosilicate was prepared by the method described by Ferdov et al.[5]. SiO_2 (14.8 g; particle size 200 μm, Merck) and 11.0 g NaOH (Junsei, Japan) were added to 200 ml of distilled water and completely dissolved by heating to boiling. Subsequently, 3.3 ml of $TiCl_4$ (Yakuri Pure Chemicals Co., Japan) hydrolyzed in 100 ml distilled water was added to the above solution. The gel obtained was then transferred into 1000 ml Teflon-lined autoclaves. The crystallization was performed under static conditions at 180 ^oC for 50 h. The reaction product was filtered and washed with deionized water and dried at 40 ^oC. H^+-titanosilicate was obtained by the ion exchange of Na^+ in Na^+-titanosilicate by H^+ using 0.1 N HCl solution. A suspension of Na^+-titanosilicate (10 g) in deionized water (200 ml) was titrated slowly with 0.1 N HCl solution to a final pH 2.0 and then maintained at this value for 24 h. H^+-titanosilicate was recovered by filtering, washing with deionized water (until Cl^- free), and drying in air at 40 ^oC.

2.2. Silica-pillared H^+-titanosilicate (SPT)

Silica-pillared H^+-titanosilicate derivatives were prepared using methods similar to those reported by Kwon et al. [14,15], which introduce TEOS and DDA into the interlayer regions of H^+-layered silicates without a separate preswelling step. Mixtures of H^+-titanosilicate, DDA (Aldrich), and TEOS (Aldrich) at molar ratios in the range 1:10:14–20 were allowed to react for 1 h at room temperature. Here, DDA molecules intercalated into H^+-titanosilicate interlayers by forming hydrogen bonds with interlayer surface Ti–OH groups. TEOS also intercalated with DDA by solvation. Mixtures at this stage were composed of DDA/TEOS co-intercalated H^+-titanosilicate gels. Unreacted DDA and TEOS were removed by vacuum filtration, which resulted in the isolating of DDA/TEOS co-intercalated H^+-titanosilicate gels. The hydrolysis of TEOS in interlayer spaces was conducted in pure water. The reaction was conducted by dispersing DDA/TEOS intercalated H^+-titanosilicate gels in deionized water at room temperature, when the viscous gray gels became white solids. Bubbles and heat were also produced at 5 min into this reaction. After soaking for 30 min, the solid products obtained were filtered, washed three times with ethanol, and oven dried at 90 ^oC. Resultant powders were siloxane-pillared H^+-titanosilicates. These powders were then heated for 5 h at 500 ^oC in air to remove template DDA, and organic by-products resulting from the hydrolysis of TEOS, to produce silica-pillared H^+-titanosilicate (SPT) derivatives.

The SPT derivatives so obtained were also then heated for 5 h at 600 or 700 °C in air to examine their thermal resistances.

2.3. Silylation of H^+-titanosilicate

DDA–OTES mixed solutions were prepared by dissolving OTES and DDA in ethanol (95%). The concentration of OTES in solution was between 0.01 and 0.1 M, and the DDA concentration was held constant at 0.1 M. H^+-titanosilicate(DDA–OTES–TS) with intercalated OTES and DDA preparation H^+-titanosilicate (0.321 g, 0.5 mmol) was then dispersed in 6 mL (0.01, 0.05, 0.1 M OTES 3 mL + 0.1 M DDA 3 mL) of these solutions (ultrasound, 20 min, at room temperature) and evaporated and dried for 24 h at 50 °C. OTES–TS was recovered by filtering, washed with ethanol until free of DDA using DDA–OTES–TS, and then dried in the air at 50 °C.

3. Characterization

X-ray diffraction data were recorded using a Bruker diffractometer using Cu K*a* radiation. The chemical compositions of Na^+-titanosilicate and H^+-titanosilicate were analyzed by energy dispersive spectroscopy (EDS; Link system AS1000-85S) and by thermo-gravimetric analysis (TGA; Dupont 9900 thermoanalyser, 10 °C/min to 900 °C, 100 ml/min N_2 purge). Scanning electron micrograph (SEM) measurements were carried out using a JEOL JSM-840A SEM. Samples, were stuck onto adhesive tape, sputter coated with gold and morphological variations were examined. Transmission electron micrographs (TEM) were obtained with a JEOL JEM-200 CX transmission electron microscope operating at 200 kV, using a thin-section technique. Powdered samples were embedded in Epoxy resin and then sectioned with a diamond knife. Microtome sectioned samples were examined. Solid-state ^{29}Si MAS NMR experiments were performed on a Bruker DSX-400 spectrometer (KBSI Daegu center, Korea) operating at 79.5 MHz. ^{29}Si MAS NMR spectra were obtained using 30-40° pulse width at a spinning rate of 6 kHz. Cross-polarization experiments were carried out with delay times of 3 s, 90° pulse of 5 s, and contact times of 2000 μs. The chemical compositions of Na^+-titanosilicate and H^+-titanosilicate were analyzed by energy-dispersive X-ray spectrometer (EDS, Link system AS1000–85S) and thermogravimetric analysis (TGA, 10 °C/min to 900 °C, 100 cm^3/min N_2 purge). The composition of the product was determined by CHN analysis (CHNS-932 (Leco)). The FT-IR spectrum was recorded on a Digilab FTS-40 FT-IR unit using the KBr disk method. Raman spectra were obtained using a Jobin Yvon/Horiba LabRAM spectrometer equipped with an integral microscope (Olympus BX 41). The 632.8 nm line of an air-cooled He/Ne laser was used as an excitation source.

4. Results and discussion

4.1. Synthesis of Na^+-titanosilicate and H^+-titanosilicate

The X-ray powder diffraction pattern of air-dried Na^+-titanosilicate, as shown in Fig. 1(a), exhibited several 00l reflections corresponding to a basal spacing of 1.08 nm. The peak

positions of this synthetic sample agreed closely with previously reported values [3,5]. Slow titration of Na^+-titanosilicate with 0.1 N HCl produced H^+-titanosilicate by exchanging Na^+ for H^+ in interlayers. The X-ray powder diffraction pattern of air-dried H^+-titanosilicate (Fig. 1(b)), exhibited 00l reflections corresponding to a basal spacing of 0.92 nm. This decrease in basal spacing relative to the Na^+ form indicates a loss of interlayer H_2O due to H^+ for Na^+ exchange. Also, the general broadening of diffraction peaks indicated that stacking disorder had occurred during this proton exchange. SEM morphologies of Na^+-titanosilicate and H^+-titanosilicate are shown in Fig. 2. Na^+-titanosilicate particles were composed of plates, and H^+-titanosilicate exhibited a similar morphology. The chemical compositions of Na^+-titanosilicate and H^+-titanosilicate were determined by TGA and EDS analysis. The TGA curve (Fig. 3(a)) indicated that air-dried Na^+-titanosilicate lost 8.5 wt% of its total initial weight as water below 200 ^oC. An additional 1.5 wt% was lost between 200 and 1000 ^oC, which was assigned to the dehydration loss of surface bound -OH groups. The chemical compositions of Na^+-titanosilicate and H^+-titanosilicate are shown in Table 1. By combining Na_2O, SiO_2, TiO_2 and weight loss, we obtained an empirical composition for synthetic Na^+-titanosilicate of $Na_4Ti_2Si_8O_{22}{\cdot}4H_2O$, which compares well with those reported previously [3-6]. H^+-titanosilicate, as shown in Fig. 3(b), showed an initial weight loss of 7.5% below 250 ^oC due to H_2O desorption, and a 6 wt% weight loss above 300 ^oC, which was attributed to the elimination of -OH groups from the structure. Based on water loss and the absence of sodium, we obtained an empirical unit cell composition of $H_4Ti_2Si_8O_{22}{\cdot}4H_2O$ or H^+-titanosilicate.

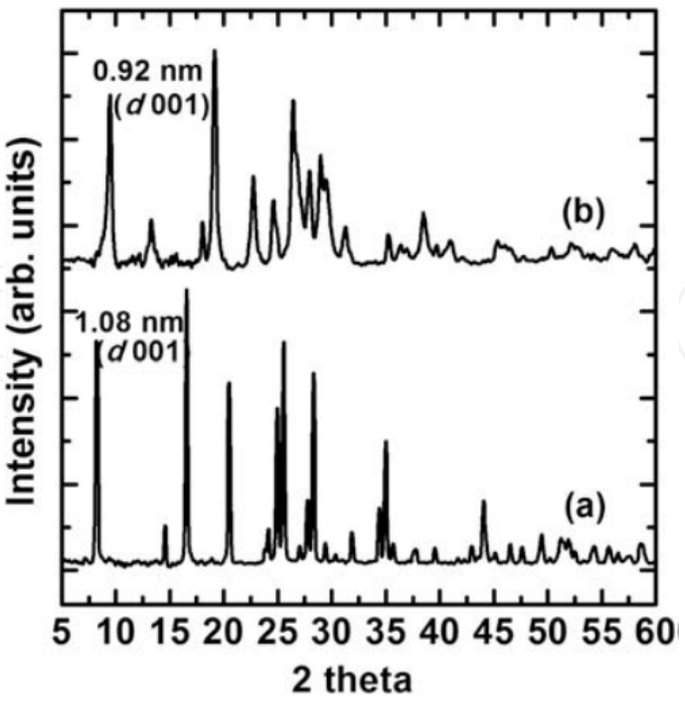

Figure 1. X-ray diffraction patterns of (a) Na^+-titanosilicate and (b) H+-titanosilicate.

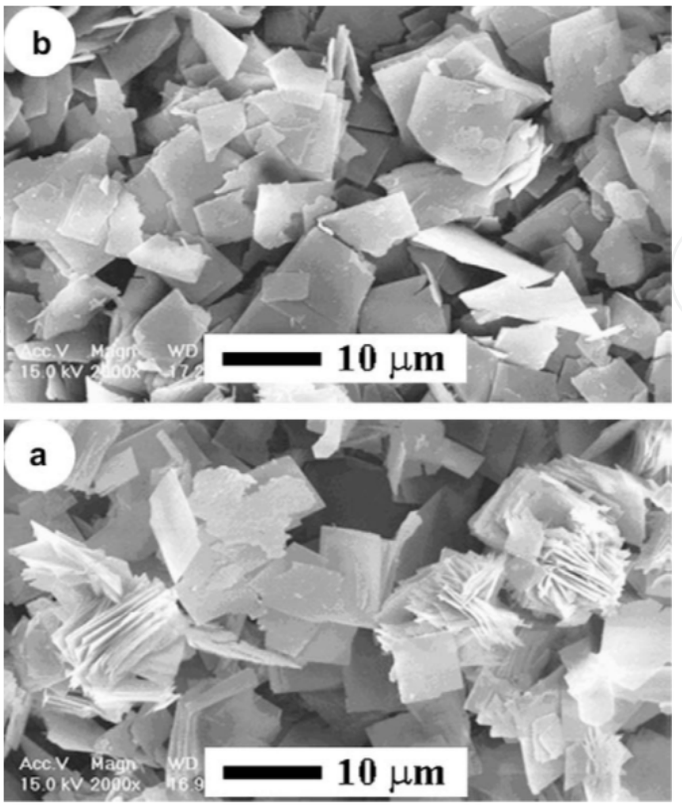

Figure 2. SEM micrographs of (a) Na^+-titanosilicate and (b) H^+-titanosilicate.

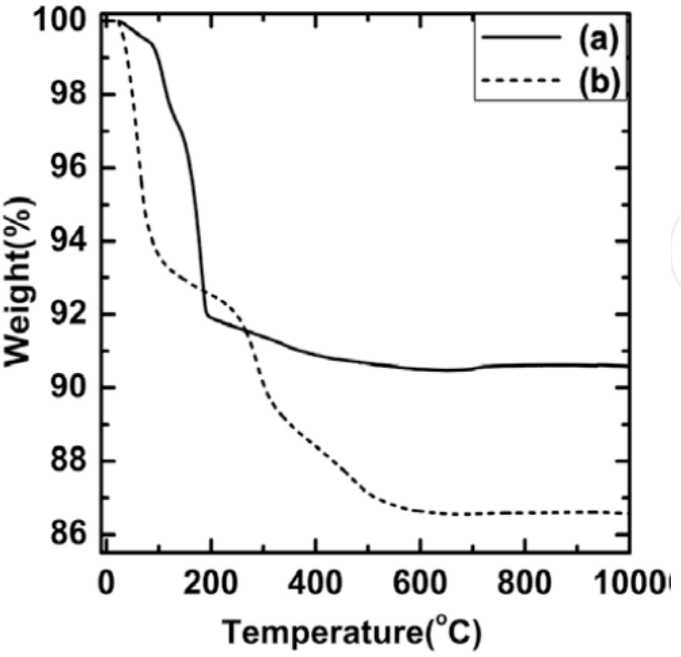

Figure 3. TGA curves of (a) Na^+- titanosilicate and (b) H^+-titanosilicate.

Samples	Weight percent				Total	Atomic ratio			
	Na_2O^a	SiO_2^a	TiO_2	H_2O		Na^a	Si^a	Ti^a	H_2O
Na^+-titanosilicate	14.80	58.50	18.20	8.50	100	3.92	8.00	1.90	3.89
HT	-	69.05	23.15	7.80	100	-	8.00	2.01	3.02

[a] EDS data. HT = H^+-titanosilicate.

Table 1. Composition of Synthetic Na^+-titanosilicate and H^+-titanosilicate

4.2. Silica-pillaring

Mixtures of H^+-titanosilicate, DDA and TEOS produced intercalation compounds in which DDA and TEOS were simultaneously intercalated into the interlayer regions. Intercalation compounds of the gel type were recovered by vacuum filtration, which allowed unreacted DDA and TEOS to be removed. The recovered gels were DDA/TEOS co-intercalated H^+-titanosilicates. In these compounds, DDA molecules between layers are solvated by TEOS molecules, which results in an additional interlayer expansion. Addition of water to the gels caused the rapid hydrolysis of TEOS in interlayer spaces. This hydrolysis occurred rapidly (within 5 min) in pure water because of the catalytic effect of DDA, and resulted in the formation of siloxane-pillared H^+-titanosilicates. The calcination of siloxane-pillared H^+-titanosilicate derivatives for 5 h at 500 ^oC resulted in the formation of silica-pillared H^+-titanosilicate (SPT) derivatives. Fig. 4 shows X-ray diffraction patterns of SPT derivatives prepared at H^+-titanosilicate:DDA:TEOS reaction stoichiometries of 1:10:14 (SPT-1), 1:10:16 (SPT-2), 1:10:18 (SPT-3) and 1:10:20 (SPT-4). SPT derivatives exhibited refractions corresponding to a basal spacing of 4.16–4.32 nm, which depended on the molar ratio of DDA to TEOS (with the exception of SPT-1). These results indicate that the molar ratio of DDA to TEOS is an important factor for successful pillaring. If the DDA/TEOS ratio is too high, the interlayer space is maintained by template DDA, and gallery TEOS cannot form a pillar firm enough between layers. Accordingly, in this situation the removal of DDA by calcination can cause the disordered collapse of interlayer spaces, which results in severe peak broadening or peak disappearance, as observed in SPT-1. Since the H^+-titanosilicate layer sheet thickness is 0.92 nm, the corresponding gallery heights are 3.24–3.40 nm, which are nearly double the chain length of DDA (1.65 nm). This implies that DDA molecules in the gallery are arranged as molecular assemblies as lamellar bilayers and that TEOS produce firm enough silica-pillars to prop the expanded gallery after the removal of DDA. Moreover, gallery height was found to increase slightly as the molar ratio of TEOS was increased. This implies that pillar size and strength depends on the quantity of gallery TEOS. The basal spacings and gallery heights of SPT derivatives are summarized in Table 2.

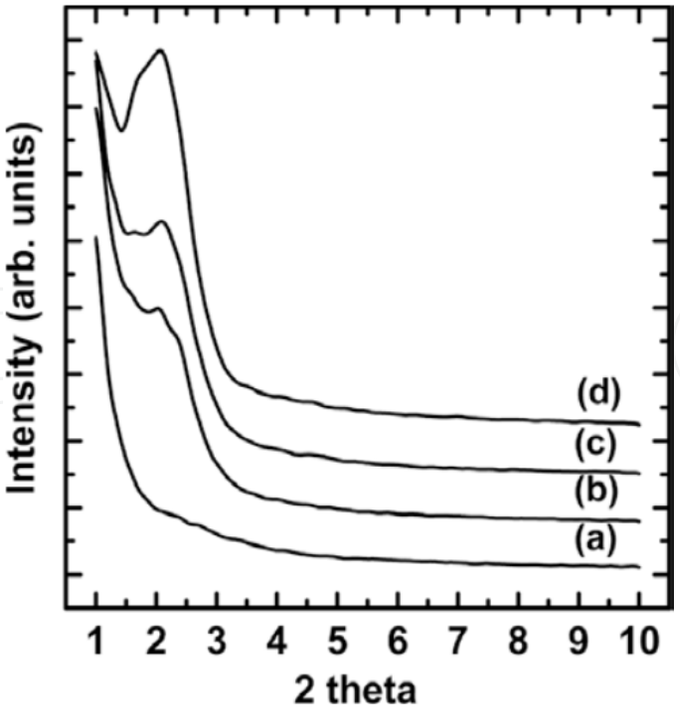

Figure 4. X-ray diffraction patterns for calcined silica-pillared H^+-titanosilicate prepared at H^+-titanosilicate:DDA:TEOS reaction stoichiometries of: (a) 1:10:14 (SPT-1), (b) 1:10:16 (SPT-2), (c) 1:10:18 (SPT-3) and (d) 1:10:20 (SPT-4).

Samples	d-spacing(nm)	S_{BET}	S_{mic}	S	H-K pore size (nm)
SPT-1	-	618	511	106	1.4
SPT-2	4.16 (3.24)	535	406	129	2.8
SPT-3	4.25 (3.33)	538	415	123	3.0
SPT-4	4.32 (3.40)	570	420	150	3.4
HT	0.92	5	-	-	

SPT = silica-pillared H^+-titanosilicate; ( ) = gallery height; gallery height = basal spacing – 0.92 nm (thickness of H^+-titanosilicate); HT = H^+-titanosilicate.

Table 2. Basal spacing, gallery heights and surface area analyses (m^2/g) for SPT products.

Fig. 5 also exhibits XRD peaks for SPT derivatives heated for 5 h at 600 or 700 °C in air. XRD peaks of SPT samples were well preserved after heat treating to 700 oC. Basal spacings and gallery heights are shown in Table 3. Basal spacing was also not altered by exposure to high temperatures. This indicates that control of DDA/TEOS ratio and the rapid hydrolysis of TEOS in water contribute to the formation of firm silica-pillars. Here, TEOS is not lost from interlayer spaces during hydrolysis, because of its waterinsolubility and rapid hydrolysis.

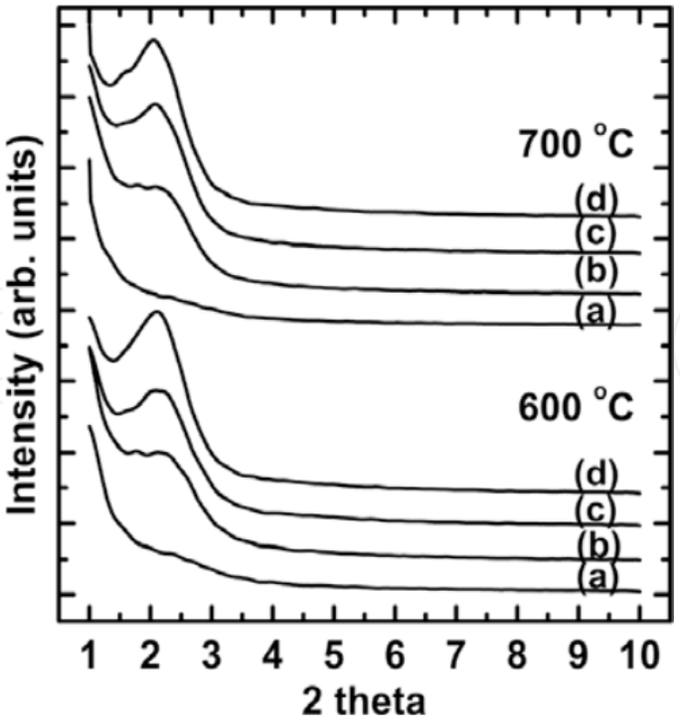

Figure 5. X-ray diffraction patterns of SPT derivatives heated for 5 h at 600 or 700 °C in air.

Typical SEM images of SPT are exhibited in Fig. 6. Most of the platelets in samples were unaffected by hydrolysis, though they swelled slightly more than H^+-titanosilicate. The small particles observed around platelets were probably broken platelets and amorphous SiO_2 caused by the hydrolysis of surface TEOS. The amount of platelet destruction was found to be related to the hydrolysis conditions used, e.g., reaction time pH of solution, and polarity of the solvent. However, this platelet destruction did not reflect SPT gallery structure destruction, probably because the gallery structure within broken platelet particles is preserved.

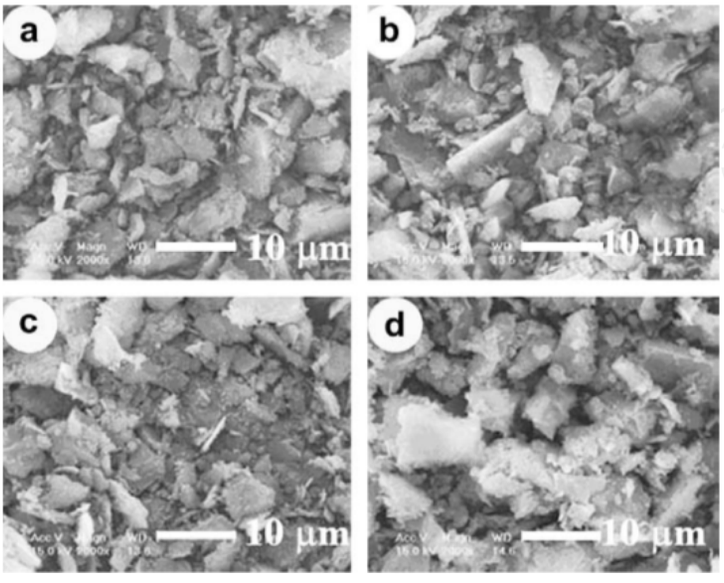

Figure 6. SEM micrographs of SPT derivatives: (a) SPT-1, (b) SPT-2, (c) SPT-3, and (d) SPT-4.

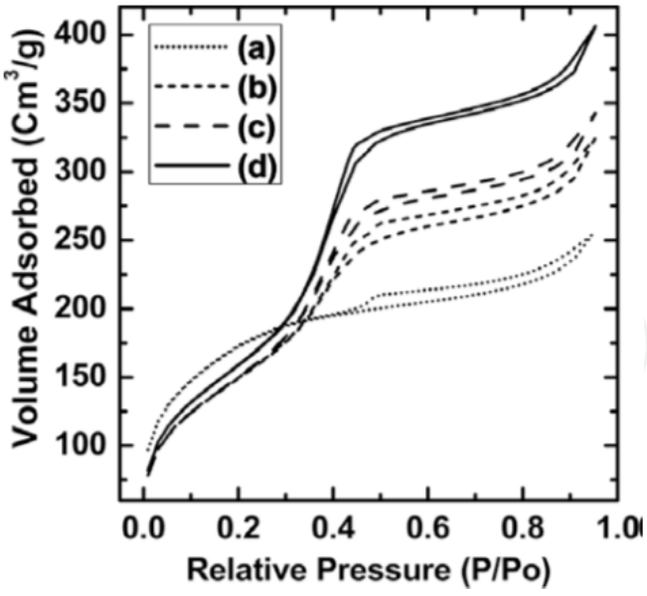

Figure 7. Nitrogen adsorption isotherms of SPT derivatives.

Fig. 7 illustrates typical N_2 adsorption/desorption isotherms for SPT. All isotherms, except for SPT-1, showed a well-defined step indicative of framework-confined mesoporosity similar to MCM-41 related materials [39]. The nearly linear portions of the adsorption curves in the partial pressure region 0.03–0.35 are also indicative of small mesopores (~0.2–3.0 nm diameter) [40]. BET surface areas and microporous and non-microporous surface areas for SPT products are summarized in Table 3. Surface areas were obtained by fitting adsorption data below $P/P_0 = 0.1$ to the BET equation [40]. H^+-titanosilicate had a total surface area of 5.0 m^2/g due to adsorption at non-porous external surfaces, but SPT products had dramatically larger total surface areas of between 535 and 618 m^2/g, which depended on the DDA/TEOS molar ratio used. Furthermore, most this surface area was attributable to the presence of micropores of <2 nm in diameter.

Samples	Basal spacing (nm)		S_{BET}	S_{mic}	S	H-K pore size (nm)
	600 °C	700 °C				
SPT-1	-	-				
SPT-2	4.14 (3.22)	4.07 (3.15)				
SPT-3	4.23 (3.31)	4.14 (3.22)				
SPT-4	4.28 (3.36)	4.22 (3.30)	551[a] 505[b]	429[a] 394[b]	122[a] 111[b]	3.2[a] 3.0[b]

S_{BET} is the N_2 BET surface area; S_{mic} and S are the microporous and nonmicroporous surface areas, respectively, obtained from *t*-plots of the nitrogen adsorption data. H-K pore size = Horvath and Kawazoe pore size (obtained from nitrogen adsorption data). [a,b]data heated at 600 °C and 700 °C, respectively.

Table 3. Basal spacing, gallery height and surface area analyses (m^2/g) for SPT derivatives heated for 5 h at 600 °C and 700 °C.

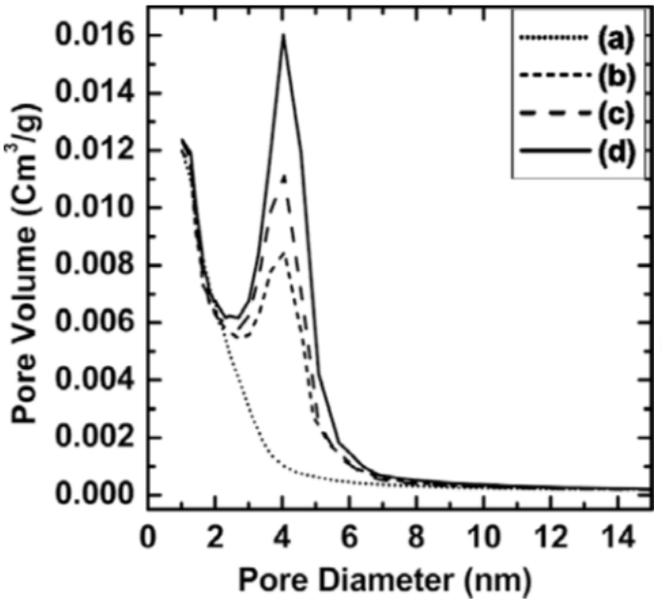

Figure 8. Pore size distributions of SPT derivatives.

Horvath and Kawazoe analysis [41] of the N_2 adsorption data (Fig. 8), yielded pore sizes of 2.8–3.4 nm, which is similar to the gallery height (3.24–3.40 nm). This indicates that DDA plays an important structure-directing role during silica-pillaring. Furthermore, pore size distributions depended to some extent on DDA/TEOS molar ratio, which reflects differences in DDA molecular assemblies in the interlayer space caused by changing DDA/TEOS molar ratios.

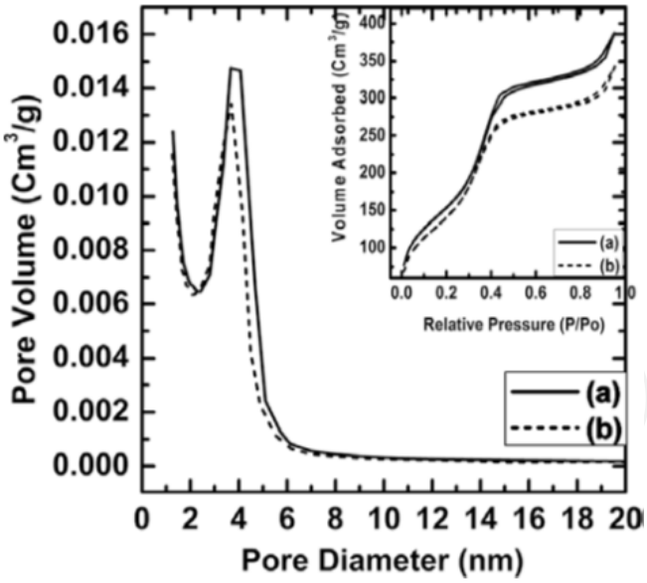

Figure 9. Pore size distributions and nitrogen adsorption isotherms of SPT-4 heated at (a) 600 °C or (b) 700 °C.

Fig. 9 shows typical isotherm and pore size distributions for SPT-4 heat treated at 600 or 700 °C. Surface areas and pore sizes are also shown in Table 3. Heat treatment hardly affected the pore size distribution and surface area of SPT-4, demonstrating the thermally stability of SPT derivatives.

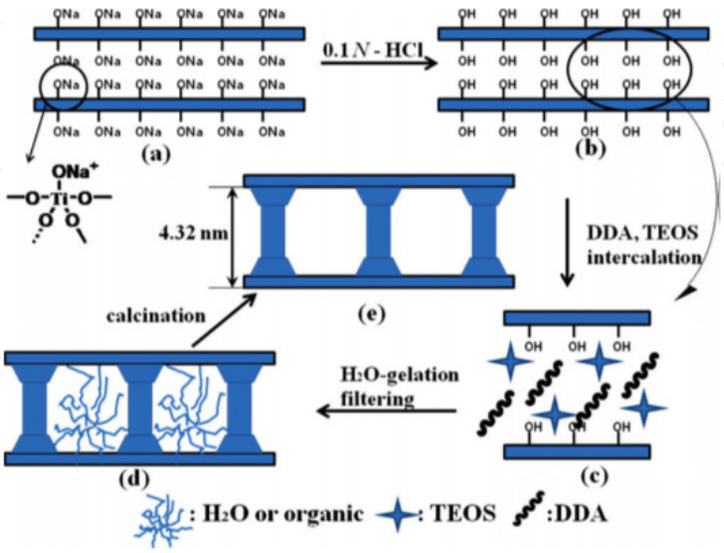

Figure 10. Schematic for the preparation of mesoporous silica-pillared H^+-titanosilicate.

Fig. 10 presents a schematic representation of mesoporous silica-pillared layered titanosilicate.

The XRD patterns of DDA–OTES–TS treated with 0.01, 0.05, 0.1 M OTES-0.1 M DDA-ethanol solution are shown in Fig. 11. Treatment of H^+-titanosilicate with the OTES–DDA mixed solution ensured successful silylation by OTES. Dried OTES–DDA–TS powder consists of H^+-titanosilicate with intercalated OTES and DDA. In the gallery, DDA changes into dodecylammonium cations [$CH_3(CH_2)_{11}NH_3^+$] as a result of the interaction with acidic silanol groups. Here, condensation between adjacent layers can not occur because of the large expansion of the interlayer space, with basal spacing between ~3.87 nm (Fig. 11(b-d)) by DDA. However, increasing concentrations of OTES broaden the reflections and decrease the basal spacing because of the high degree of grafting that reduces the amount of intercalated DDA. The XRD patterns of DDA–OTES–TS after washing with ethanol to remove the DDA showed that an increasing concentration of OTES broadened the reflections and decreased the basal spacing, because a high degree of grafting reduces the amount of intercalated OTES (Fig. 11(e-g)). The interlayer space had a basal spacing of ~2.95 nm (Fig. 11(e-g)). This small increase in basal spacing indicates that OTES molecules arrange with paraffin-type in the gallery.

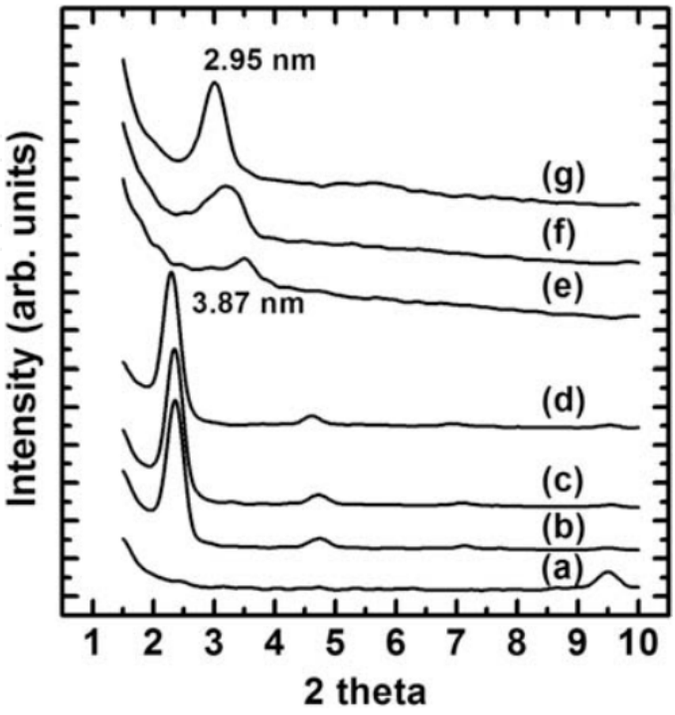

OTES–TS, (c) 0.1 M DDA-0.05 M OTES–TS, (d) 0.1 M DDA-0.1 M OTES–TS, (e) 0.01 M OTES–TS, (f) 0.05 M OTES–TS and (g) 0.1 M OTES–TS.

Figure 11. XRD patterns of (a) as-prepared H^+-titanosilicate, (b) 0.1 M DDA-0.01 M

The FT-IR spectrum of H^+-titanosilicate and OTES–TS is shown in Fig. 12. The band at 1469 cm^{-1} has been assigned to the asymmetric $–CH_3$ deformation of $–Si–CH_3$ [42,43], while the 2852, 2922 and 2960 cm^{-1} bands corresponded to $–CH_2CH_3$. The –OH stretching band is seen at 3208 cm^{-1} in –OH form and the H_2O bending vibration is seen at 1619 and 1645 cm cm^{-1}. In the OTES–TS spectrum, the absorption band from the Si–O–Si type of motion overlaps with strong Si–O–Ti absorption bands at 586 and 866 cm^{-1}. However, additional bands were observed at 631, 699, 776, 909, 1054, 1149 cm^{-1} in the OTES–TS spectra. These bands were also observed in the spectrum of titanosilicate [44–47] and probably arose from Ti–O–Si linkages formed by silylation. The bonding of the alkylsilyl groups with the silicate layers was revealed by the Raman spectra (Fig. 13). Titanosilicate is composed of $–(Si–O)_4–Ti–O–$ units with their Si-O-Si environments observed at around 600 cm^{-1}, Ti–O–Si: 960 cm^{-1} and –OH: 970, 1100, 3600 cm^{-1} [48–51]. The reaction products exhibit Raman bands at 223, 328, 385, 429, 477, 600, 920, 1029, 1078 and 1301 cm^{-1}, respectively. The spectra also showed a substantial increase in the relative intensity of Ti–O–Si signals due to the increase in formed Ti–O–Si units by the silylation of interlayer Ti–OH groups.

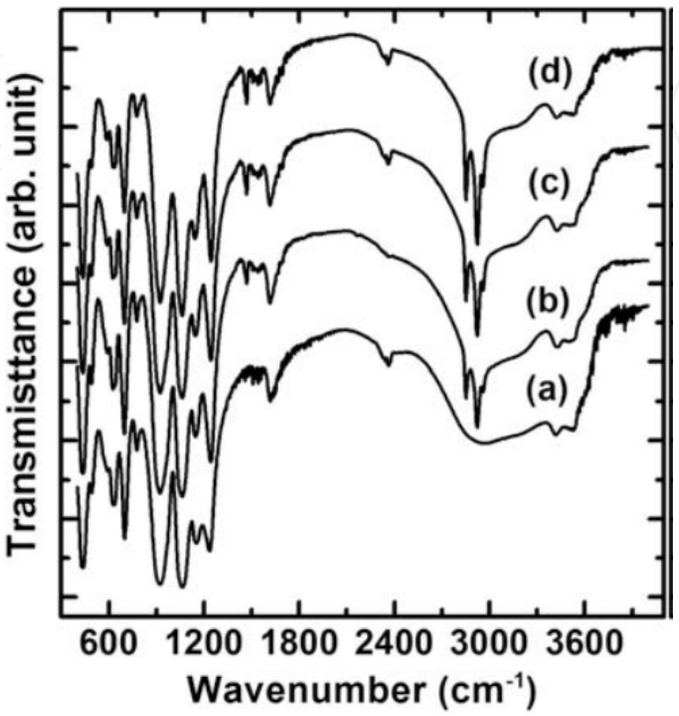

Figure 12. FT-IR spectra of (a) as-prepared H^+-titanosilicate, (b) 0.01 M OTES–TS, (c) 0.05 M OTES–TS and (d) 0.1 M OTES–TS.

TGA data from DDA–OTES–TS and insert of OTES–TS treated in N_2 at a heating rate of 10 ^oC/min are shown in Fig. 14. The weight loss of DDA–OTES–TS in the temperature range from 100 to 250 ^oC was ~23.0 wt.% and was probably caused by water and DDA contained between the interlayers. A weight loss of ~25 wt.% was recorded between 250 and 650 ^oC, because the TS surface organic chains group was thermally cracked in this temperature range (Fig. 14). These values represent the loadings of organic functions on OTES–TS and are in agreement with the C, H, N contents of 9.4–20.6 wt.% obtained by chemical analysis. The composition of the products determined by the C, H, N analysis is summarized in Table 1. The C, H, N content in OTES–TS increased with increasing OTES concentration. The C content in DDA–OTES–TS decreased with increasing OTES concentration because DDA adsorption decreases at higher OTES content. The almost constant N content indicates that the sum of OTES and DDA remain nearly independent from the degree of silylation.

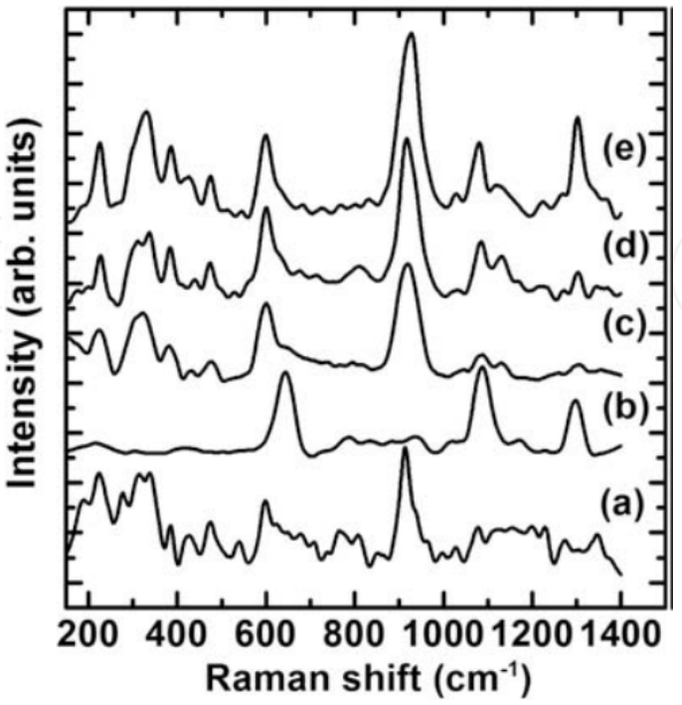

Figure 13. Raman spectra of (a) as-prepared H^+-titanosilicate, (b) OTES, (c) 0.01 M OTES–TS, (d) 0.05 M OTES–TS and (e) 0.1 M OTES–TS.

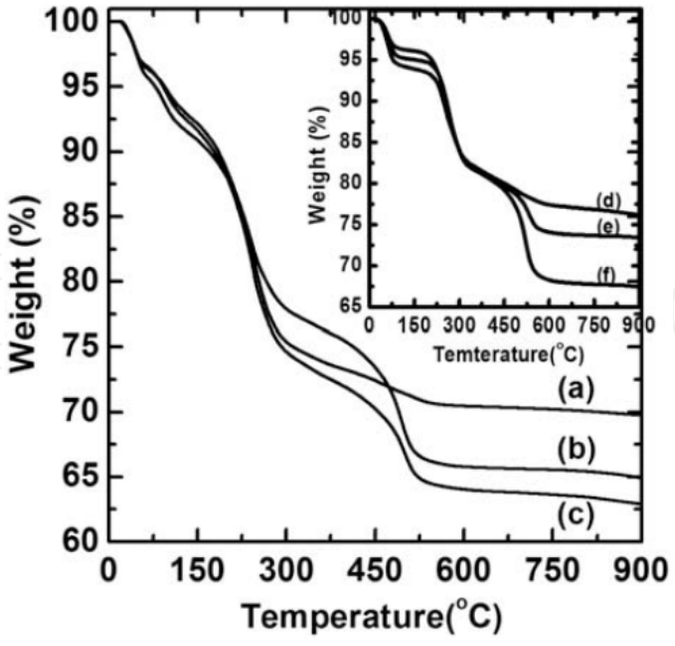

Figure 14. TGA of (a) 0.1 M DDA-0.01 M OTES–TS, (b) 0.1 M DDA-0.05 M OTES–TS, (c) 0.1 M DDA-0.1 M OTES–TS, (d) 0.01 M OTES–TS, (e) 0.05 M OTES–TS, (f) 0.1 M OTES–TS.

Silylated-TS	Composition Weight Percent				
	C [1)]	H [1)]	N [1)]	CHN [2)]	SiO_2, TiO_2 (%)
0.10 M DDA-0.01 M OTES	16.80	3.55	1.75	20.1	77.9
0.10 M DDA-0.05 M OTES	22.08	4.27	1.92	25.2	71.73
0.10 M DDA-0.10 M OTES	23.05	4.80	1.67	29.0	70.48
0.01 M OTES [3)]	9.38	2.65	0.81	1.4	87.16
0.05 M OTES [3)]	14.53	3.45	0.99	7.1	81.03
0.10 M OTES [3)]	20.60	4.00	1.08	14.2	74.32

[1)] Evaluated by CHN analysis
[2)] Evaluated by CHN calculation (Contains CHN of 0.1M DDA, 0.01, 0.05, 0,1M-OTES)
[3)] Washed with EtOH

Table 4. Chemical composition of silylated titanosilicate.

The solid-state ^{29}Si MAS NMR spectra for silylated H^+-titanosilicate show Q^3 (-105.7 ppm), Q^4 (-110 to -112 ppm), and T^2 (-50 to -60 ppm) signals with diverse environments of silicon (Fig. 15). The increase of the Q^3/Q^4 ratio compared with H^+-titanosilicate clearly indicates the grafting of OTES molecules to the surface silanol groups. The new peaks (T^2) near -59.5 ppm, in 0.1 M OTES–TS were attributed to the Si atoms of the grafted OTES molecules. In general, Si atoms of the silicate network exhibited signals (Q^3 and Q^4) in the range of -102 and -112 ppm, whereas Si atoms in the silylating agent grafted to the surface showed signals (T^2) at -50 to -60 ppm. Caravajal et al. [52], Impens et al. [53], Lin et al. [43] and D'Amore and Schwarz [54] all reported the mechanism and solid NMR data for the silylation of amorphous silica, alumina and Ti-MCM-41 with alcoxysilane. The Si signals for OTES silylated on silica was in the range of -49 to -68 ppm, depending upon the bonding type. Caravajal et al. [55] and Shimojima et al.[30] also showed that Si signals for alkyltrichlorosilane grafted on kanemite appeared between -56 and -65 ppm. The signals from 0.5 M DDA-0.1 M OTES–TS were similar to signals of kanemite silylated by alkyltrichlorosilane. The TEM image (Fig. 16) explains the reason why OTES–TS samples, in spite of partial destruction of platelets in the outer appearance in the SEM, exhibit uniform distance distributions and ordered basal spacing. The crosssection of an OTES–TS platelet shows several silicate sheets with uniform spacing of ~2.95 nm. A hypothetical diagram for the silylation by OTES and the intercalation of DDA during the evaporation of the solvent is shown in Fig. 17. The evaporation of ethanol starts at the outside of the particles, resulting in a higher concentration of DDA and OTES on the external surface and subsequently promoting the intercalation of OTES and DDA (Fig. 17(b and c)). The evaporation of residual ethanol in the gallery results in the silylation of OTES (Fig. 17d). The water molecules contained in ethanol catalyze the interlayer surface silylation of OTES during the evaporation of ethanol. The condensation of alkoxysilane is known to be catalyzed by bases. DDA as a gallery expander can also play a role as catalyst for the grafting of OTES into the surface silanol groups.

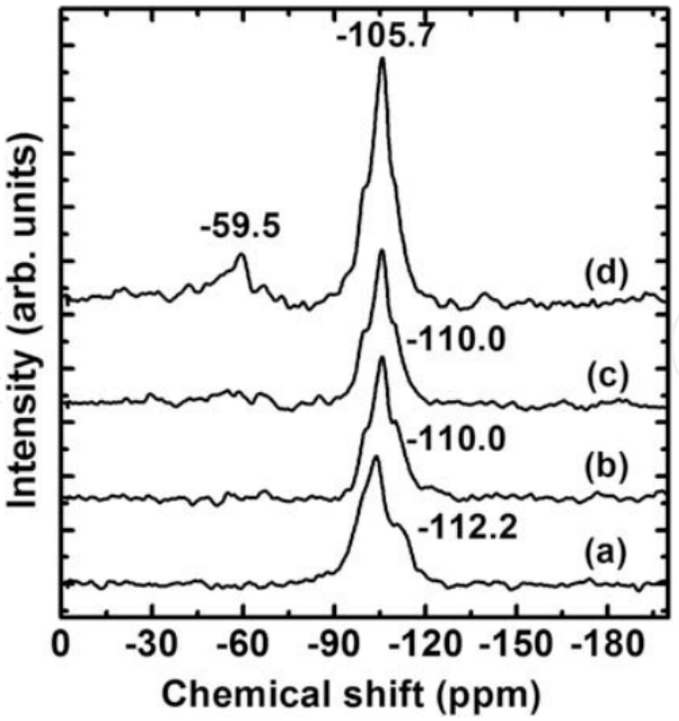

Figure 15. ^{29}Si MAS NMR spectra of (a) as-prepared H^+-titanosilicate, (b) 0.01 M OTES– TS, (c) 0.05 M OTES–TS and (d) 0.1 M OTES–TS.

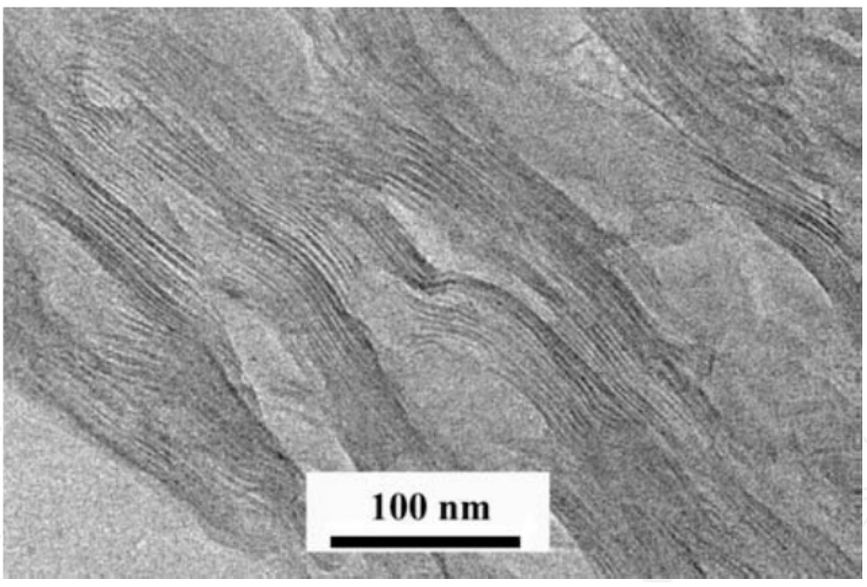

Figure 16. Transmission electron micrographs for OTES–TS.

The narrow pore size distributions (~0.7 nm peak width at half peak maximum) of SPT derivatives are similar to those of the related MCM-41 (~0.5 nm peak width), which is produced using a surfactant template [39]. This indicates that DDA molecules play a decisive role in pore formation in SPT derivatives, and that they form molecular assemblies similar to those formed by surfactant micelles. An optimal DDA/TEOS molar ratio in interlayer regions could afford near ideal conditions for the formation of micellar neutral amine assemblies, and such conditions favor the DDA-templated hydrolysis of TEOS. Tanev and Pinnavaia [56]

demonstrated that the assembly of hexagonal mesoporous metal oxides can also be achieved by hydrogen bonding between neutral amine and TEOS. In porous materials formed by this gallery-templated reaction, specific surface areas are composed of the surfaces of micropores, where pore walls act as pillars and mesopores. Therefore, the lateral spacing between pillars in conventional pillared layered materials is not the sole contributor to increased microporosity.

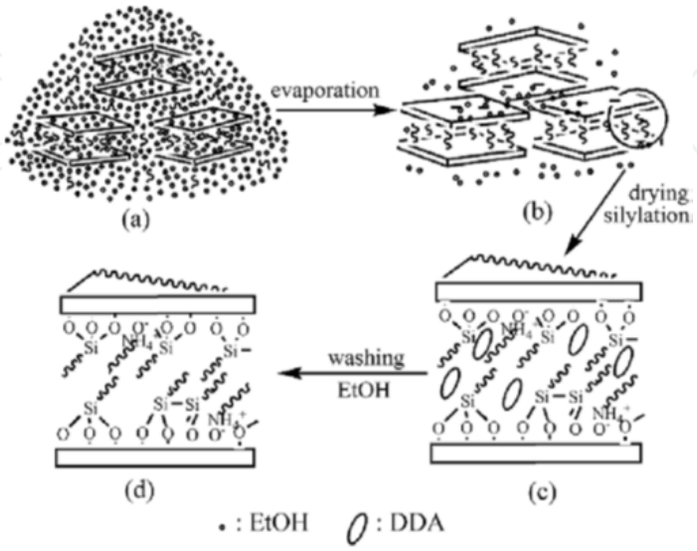

Figure 17. Schematic representation of the intercalation and silylation of DDA and OTES for H^+-titanosilicate.

SPT derivatives exhibit a broad pore size distribution as compared with MCM-41. Furthermore, they offer new opportunities for the rational design of heterogeneous catalyst systems because of their complementary chemical functionality, thermal stability, and stable pore size distribution to the small mesopore range (1.0–2.0 nm). In addition, the existence of five-coordinated titanium(V) in the interlayer surfaces of SPT derivatives makes then promising potential oxidation catalysts.

5. Conclusion

The simultaneous intercalation of DDA and TEOS into H^+-titanosilicate interlayers and subsequent intragallery DDA-catalyzed hydrolysis of TEOS resulted in mesoporous silica-pillared H^+-titanosilicate (SPT) derivatives. These derivatives exhibited refractions corresponding to a basal spacing of 4.16–4.32 nm, a uniform pore size of 2.8–3.4 nm and large surface areas of 535–618 m^2/g. The structural and physical properties of SPT derivatives exhibited excellent thermal resistance, i.e., they remained stable after heating for 5 h at 700 ^oC in air. Our results indicate that DDA plays a decisive role in pore formation, because it acts as a base catalyst and as a micelle-like template during the hydrolysis of TEOS. In particular, the rapid hydrolysis of TEOS in water controls TEOS outflow from interlayers and contributes to the formation of firm silica-pillars.

Our results show that intercalation and silylation proceeded more effectively by the evaporation of solvents than by filtration and drying. This evaporation process should be a

very efficient method for the intercalation and silylation of silane coupling agents into layered compounds and organic–inorganic materials.

Author details

Kyeong-Won Park
Department of Chemistry and Research Institute of Natural Science, Gyeongsang National University, Republic of Korea

6. References

[1] J. Rocha, M.W. Anderson, Eur. J. Inorg. Chem. (2000) 801.
[2] Z. Lin, J. Rocha, P. Brandao, A. Ferrira, A.P. Esculcas, J.D. Pedrosa de Jesus, A. Philippou, M.W. Anderson, J. Phys. Chem. 101 (1997) 7114.
[3] H. Du, M. Fang, J. Chen, W. Pang, J. Mater. Chem. 6 (1996) 1827.
[4] M.A. Roberts, G. Sankar, J.M. Thomas, R.H. Jones, H. Du, M. Fang, J. Chen, W. Pang, R. Xu, Nature 381 (1996) 401.
[5] R. Murugavel, H.W. Roesky, Angew. Chem., Int. Ed. Engl. 36 (5) (1997) 477.
[6] S. Ferdov, V. Kostov-kytin, O. Petrov, Chem. Commun. (2002) 1786.
[7] V. Kostov-kytin, B. Mihailova, S. Ferdov, O. Petrov, Solid State Sci. 6 (2004) 967.
[8] M.E. Landis, B.A. Aufdembrink, P. Chu, I.D. Johnson, G.W. Kirker, M.K.J. Rubin, J. Am. Chem. Soc. 113 (1991) 3189.
[9] J.S. Daily, T.J. Pinnavaia, Chem. Mater. 4 (1992) 855.
[10] E. Ruitz-Hitzky, J.M. Rojo, Nature 287 (1980) 28.
[11] S.Y. Jeong, O.Y. Kwon, J.K. Seo, H. Jin, J.M. Lee, J. Colloid Interf. Sci. 175 (1995) 253.
[12] O.Y. Kwon, S.Y. Jeong, J.K. Seo, B.H. Ryu, J.M. Lee, J. Colloid Interf. Sci. 177 (1996) 677.
[13] A. Galarneau, A. Barodawalla, T.J. Pinnavaia, Nature 374 (1995) 529.
[14] O.Y. Kwon, J. Ind. Eng. Chem. 5 (1999) 314.
[15] O.Y. Kwon, H.S. Shin, S.W. Choi, Chem. Mater. 12 (2000) 1273.
[16] K.W. Park, S.Y. Jeong, O.Y. Kwon, Appl. Clay Sci. 27 (2004) 21.
[17] K.W. Park, O.Y. Kwon, J. Ind. Eng. Chem. 10 (2004) 252.
[18] K.W. Park, O.Y. Kwon, Bull. Korean Chem. Soc. 25 (2004) 965.
[19] Michael E. Landis, B.A. Aufdembrink, P. Chu, I.D. Johnson, G.W. Kirker, M.K. Rubin, J. Am. Chem. Soc. 113 (1991) 3189.
[20] J.S. Daily, T.J. Pinnavaia, Chem. Mater. 4 (1992) 855.
[21] M. Ogawa, K. Kuroda, Bull. Chem. Soc. Jpn. 70 (1997) 2593.
[22] Soon-Yong Jeong, Oh-Yun Kwon, Jeong-Kwon Suh, Hangkyo Jin, Jung Min Lee, J. Colloid Interface Sci. 175 (1995) 253.
[23] Oh-Yun Kwon, Soon-Yong Jeong, Jeong-Kwon Suh, Beyong-Hwan Ryu, Jung-Min Lee, J. Colloid Interface Sci. 177 (1996) 677.
[24] O.Y. Kwon, S.W. Choi, Bull. Korean Chem. Soc. 20 (1999) 69.

[25] O.Y. Kwon, H.S. Shin, Chem. Mater. 12 (2000) 1273.
[26] O.Y. Kwon, K.W. Park, J. Ind. Eng. Chem. 7 (1) (2001) 44.
[27] A. Galarneau, A. Barodawalla, T.J. Pinnavaia, Nature 374 (1995) 529.
[28] E. Ruiz-Hitzky, J.M. Rojo, Nature 287 (1980) 28.
[29] E. Ruiz-Hitzky, J.M. Rojo, Colloid Polym. Sci. 287 (1985) 28.
[30] A. Shimojima, D. Mochizuki, K. Kuroda, Chem. Mater. 13 (2001) 3603.
[31] S. Okutomo, K. Kuroda, M. Ogawa, Appl. Clay Sci. 15 (1999) 253.
[32] M. Ogawa, S. Okutomo, K. Kuroda, J. Am. Chem. Soc. 120 (1998) 7361.
[33] T. Yanagisawa, K. Kuroda, C. Kato, React. Solid 5 (1988) 167.
[34] P.H. Thiesen, K. Beneke, G. Lagaly, J. Mater. Chem. 12 (2002) 3010.
[35] M.W. Weimer, H. Chen, E.P. Giannelis, D.Y. Sogah, J. Am. Chem. Soc. 121 (1999) 1615.
[36] Kostas S. Triantafyllidis, Peter C. LeBaron, In Park, Thomas J. Pinnavaia, Chem. Mater. 18 (2006) 4393.
[37] Hao Fong, Richard A. Vaia, Jeffrey H. Sanders, Derek Lincoln, Peter J. John, Andrew J. Vreugdenhil, John Bultman, Clifford A. Cerbus, Hong G. Jeon, Polymer Prepr. 42 (1) (2001) 354.
[38] S. Solarski, S. Benali, M. Rochery, E. Devaux, M. Alexandre, F. Monteverde, P. Dubois, J. Appl. Polymer Sci. 86 (2004) 238.
[39] C.T. Kresge, M.E. Leonowicz, W.J. Roth, J.C. Vartuli, J.S. Beck, Nature 359 (1992) 710.
[40] S. Brunauer, P.H. Emmett, E. Teller, J. Am. Chem. Soc. 60 (1938) 309.
[41] G. Horvath, K.J. Kawazoe, Chem. Eng. Jpn. 16 (1983) 470.
[42] Jie Bu, Hyun-Ku Rhee, Catal. Lett. 65 (2000) 141.
[43] K. Lin, L. Wang, F. Meng, Z. Sun, Q. Yang, Y. Cui, D. Jiang, F-S. Xiao, J. Catal. 235 (2005) 423.
[44] Damodara M. Poojary, Roy A. Cahill, Abraham Clearfield, Chem. Mater. 6 (1994) 2364.
[45] Yunling Liu, Hongbin Du, Feng-Shou Xiao, Guangshan Zhu, Wenqin Pang, Chem. Mater. 12 (2000) 665.
[46] Elizabeth A. Behrens, Damodara M. Poojary, Abraham Clearfield, Chem. Mater. 8 (1996) 1236.
[47] Yining Huang, Zhimei Jiang, Wilhelm Schwieger, Chem. Mater. 11 (1999) 1210.
[48] Yali Su, Mari Lou Balmer, Bruce C. Bunker, J. Phys. Chem. B 104 (2000) 8160.
[49] Goutam Deo, Andrzej M. Turek, Israel E. Wachs, Zeolites 13 (1993) 365.
[50] R.H. Stolen, G.E. Walrafen, J. Chem. Phys. 64 (1976) 2623.
[51] Vladislav Kostov-Kytin, Boriana Mihailova, Stanislav Ferdova, Ognyan Petrov, Solid State Sci. 6 (2004) 967.
[52] G. Stephen Caravajal, Donald E. Leyden, Gregory R. Quinting, Gary E. Maciel, Anal. Chem. 60 (1988) 1776.
[53] N.R.E.N. Impens, P. van der Voort, E.F. Vansant, Micropor. Mesopor. Mater. 28 (1999) 217.
[54] M.B. D'Amore, S. Schwarz, Chem. Commun. (1999) 121
[55] G.S. Caravajal, D.E. Lyden, G.R. Quinting, G.E. Maciel, Anal. Chem. 60 (1988) 1776.
[56] P.T. Tanev, T.J. Pinnavaia, Science 267 (1995) 865.